Experimental Study of the Hypersonic Turbulent Boundary Layer on a Cold Slender Cone

Z. B. Lin*
Chinese Academy of Science, Beijing, China
and
J. K. Harvey†
Imperial College, London, England, United Kingdom

This paper presents measurements of both the mean and time-resolved properties of a naturally turbulent boundary layer on a highly cooled sharp cone in hypersonic flow. The experiments were carried out on a 5 deg half-angle cone at zero angle of attack in a Mach 9.26 flow in a gun tunnel. The unit Reynolds number was 4.4×10^7/m and the wall-to-stagnation temperature ratio was 0.273. Conventional surface and flow field instrumentation, including a new compact fast responding total temperature probe, was used to acquire time-averaged data. Measurements of the mean and the fluctuating density within the boundary layer are included that were obtained using the electron beam fluorescence technique. Comparisons are made between the measured data and several laws applicable to low-Mach-number zero-pressure-gradient boundary layer flows. It is shown that measured data are correlated by the van Driest extension to the Crocco relationship and agree with the velocity defect law modified by Fernholz.[1] As expected, the mixing length concept is shown to be too simple to predict the density fluctuation correctly for this flow. Fluctuation spectra differ from the result from incompressible flows. The spatial correlation of the fluctuations emphasizes that there is considerable energy in the small eddies.

Nomenclature

C_f = skin friction coefficient = $\tau_w/\frac{1}{2}\rho_\infty u_\infty^2$
H_{i2} = shape factor = δ_i/δ_2; $i = 1,3,4$
ℓ = mixing length
M = Mach number
p = pressure
Pr = Prandtl number
p_t = pitot pressure
$\dot{q}$ = heat transfer rate
r = recovery factor = 0.89
Re = Reynolds number
Re_θ = Reynolds number = $(\rho_e u_e/\mu_e)_{\delta_2}$
$Re_{\theta 2}$ = Reynolds number = $(\rho_e u_e/\mu_w)_{\delta_2}$
St = Stanton number = $\dot{q}/\rho_e u_e c_p(T_r - T_W)$
T = temperature
T_r = recovery temperature
u = velocity
$\bar{u}^*$ = transformed velocity
u_τ = friction velocity = $(\tau_w/\rho_w)^{1/2}$
x,y = coordinate axes
δ_p = boundary-layer thickness at $p_t/p_{te} = 0.99$
δ^* = δ_1 displacement thickness
θ = δ_2 momentum defect thickness
δ_3 = kinetic energy defect thickness
δ_4 = total enthalpy defect thickness
γ = ratio of specific heats = c_p/c_v
ρ = density
Δ^* = length parameter
τ_w = shear stress at wall
ϵ = eddy viscosity

Subscripts
e = boundary-layer edge conditions
w = wall conditions
o = stagnation conditions
aw = adiabatic wall
∞ = freestream

Introduction

ALTHOUGH it is about 100 years since Reynolds published his famous paper, many aspects of the subject of turbulence remain sketchily understood. This is especially true in the hypersonic regime where our knowledge of transition and the subsequent development of the turbulent flow can only be said to be poor. This arises in part because of the paucity of good measured data caused by the difficulties experienced in conducting accurate experiments at high Mach numbers. Fresh problems are thought to arise from the fundamental change that occurs in the character of the boundary layer when the Mach number rises above about seven. Fluctuations in the static thermodynamic quantities such as density and temperature, which in most low-speed flows are small enough to be neglected, increase in parts of the flow, to a point where they are the most significant varying properties. Furthermore, transition becomes an extended process taking many boundary-layer thicknesses to complete. The resulting nominally turbulent boundary layer carries with it an imprint of the upstream history, and it takes a long time for it to adjust to what may be considered to be an equilibrium form. For these and other reasons, the flows differ fundamentally from those at lower speeds. These changes exacerbate efforts to extend to higher Mach number the prediction methods that have been successfully developed for low-speed flows.

Because of the possible differences in turbulent layer structures, experiments are needed to establish a basic physical picture of the hypersonic turbulent boundary layer. Much of the available experimental data have been obtained on wind-tunnel walls, where long lengths of flow are available to generate fully developed equilibrium boundary layers. However,

Presented as Paper 87-1513 at the AIAA 22nd Thermophysics Conference, Honolulu, HI, June 8-10, 1987; received Aug. 12, 1987; revision received Feb. 22, 1988.

*Senior Research Scientist, Institute of Mechanics.
†Reader in Gas Dynamics, Department of Aeronautics. Member AIAA.

differences that are thought to be attributable to the upstream histories have been observed between these boundary layers and those developed on bodies. The nozzle boundary layers may well not be representative of those relevant to practical flight conditions. On the other hand if a boundary layer is studied on a body it is often necessary to induce transition artificially with a trip. It is observed that the fluctuation levels within these turbulent boundary layers do not approach those of the naturally turbulent layer until some long time after transition is apparently complete. It is thus important to make sure that a boundary layer to be studied is either naturally turbulent or that sufficient distance is allowed after tripping for an equilibrium layer to develop.

In this study, a naturally turbulent boundary layer has been investigated, which formed on the cold wall of a sharp slender cone model at zero angle of attack. The ratio T_w/T_{oe} was 0.273. The experiment has been conducted in two phases. Firstly, the time-averaged properties of the boundary layer downstream of transition have been obtained from a pitot pressure survey taken in conjunction with measurements of wall heat transfer, surface static pressure, and skin friction inferred from Preston tubes. Corresponding total temperature measurements made on the cone model in the same flow and reported independently by Wang and Hillier[2] are used with the pitot pressure data to calculate the mean velocity profiles. This first phase forms a basis for the second in which measurements of the mean and fluctuating density and correlations of the latter have been obtained using the electron beam fluorescence technique. This is a nonintrusive method in which a narrow electron beam is fired into the gas. The density is inferred from observing the resulting ultraviolet fluorescence. The method has an inherent high-frequency response and is able to resolve details of the turbulent structure. Application of the technique to a flow where the density levels were high enough to ensure natural transition was new and required significant improvements to the experimental equipment that previously had been limited to low-density investigations. The experiment demonstrated that useful results can be obtained using this technique.

Experiment

The experiments were performed in the Imperial College No. 2 gun tunnel. This facility is a conventional intermittent blowdown wind tunnel with a contoured 0.4 m diam Mach 9.26 axisymmetric nozzle fed by a free-piston compression heater. Operating at the highest driver pressure of 1000 atm, a unit Reynolds number of 4.4×10^7/m based on freestream conditions is achieved with the flow total temperature equalling 1064 K. Steady test conditions last for about 5 ms.

Two smooth sharp 5 deg cone models were used for the test. They were both 1.0 m long and they were mounted so as to be completely within the uniform flow region of the test flow. One of the models was designed to house the electron beam gun used for the fluorescence measurements, and the other was equipped with conventional probe and surface instrumentation. The external shape and method of mounting the two models was identical.

Most of the pitot pressure data were obtained using a probe in which a Kulite miniature piezoelectric-resistor transducer was directly fitted. The tip of the probe was shaped like a wedge of small angle with an entrance height less than 1% of the thickness of boundary layer. The intake was shaped to match the curvature of the model's surface. High spatial resolution was achieved with rapid response. The data near the outer edge of the boundary layer were obtained using a less sensitive strain gage transducer and the entrance of this probe was less than 7% of boundary-layer thickness. Similar transducers were used for the surface pressure measurements.

Preston tubes were used to measure the surface impact pressure distribution from which skin friction values were estimated using appropriate empirical calibration curves. Two circular probes of 1.25 and 2.07 mm diam were used with the piezoelectric transducer to perform these tests.

Heat transfer was measured with thin-film platinum gages that were mounted on the cone model along a generator from the apex. The platinum gages were made either by painting or by evaporation through a mask onto 3 mm diam polished quartz substrates. Each sensor had the same curvature as that of the local cone surface, and its position was adjusted to ensure that it was exactly flush with the cone.

The total temperature probes were of a miniature thermocouple type with an unheated vented shield. Chromel-alumel sensor wires, 12.5 μm in diameter and 2.4 mm long, were soldered between two 0.1 mm diam support prongs. Calibration of the probes covered an appropriate range of Reynolds number to embrace the values encountered in the boundary layer surveys. The design was optimized to ensure that steady measurements of total temperature were achieved well within the 5 ms test period. The spatial resolution was determined by the intake dimensions, which were about 0.8 mm high by 1.5 mm wide. A high ratio of sensor-to-total temperature ratio, typically 0.9, was obtained with this probe design. This helped to minimize the error commonly encountered with this type of probe when a large correction factor has to be applied to the measured data. Further details of these probes are given in Wang and Hillier.[2]

All signals from these instruments were amplified, passed through a 1 KHz low pass filter, and then recorded by the gun tunnel digital data acquisition system. The maximum error in the measured quantities are: $\pm 0.1\%$ of δ_t in probe position relative to the surface, $\pm 2\%$ in pitot pressure P_t, $\pm 5\%$ in total temperature T_o, $\pm 7\%$ in heat transfer $\dot{q}_w$, and $\pm 3\%$ in both static pressure p_e and impact pressure.

The mean and fluctuating density measurements presented in this paper were obtained using the electron beam technique. In this experiment a narrow beam of high-energy electrons was passed through the pure nitrogen test flow and the resulting glow in the $N_2(2+)$ band observed at selected points along the beam's path with an appropriate optical system incorporating fast responding photomultiplier detectors. The intensity of the emitted light relates to the density of the test gas at the point where the observation is being made. Despite its complexity the method has advantages over others such as hot-wire anemometry in being nonintrusive and inherently very quick to respond. It is possible to measure spatial correlations within the boundary layer without probe interference by taking simultaneous observations at several points along the beam's path or by using multiple beams.

The model was constructed in three sections. The final section was made from nonmagnetic stainless steel and housed a miniature electron gun. The model was supported by a rigid hollow sting that also served as a duct for the vacuum, focusing magnet coil cooling water and electrical services to the gun.

An accelerating voltage of 50 KV was used with a maximum beam input current of 2 mA. A unique feature of the gun was the advanced design single electromagnet that focused the beam to a very small diameter (about 50 μm). The beam itself was used to drill a fine hole through a diaphragm, located at the cone surface, which isolated the cathode cavity from the test gas. Using this novel technique it was possible to maintain a vacuum of better than 10^{-4} Torr within the gun with an external pressure of 110 Torr.

The optical system used to record the intensity of the fluorescence consisted of a 40-mm-diam lens (f = 125 mm), a front-surfaced mirror coated to give maximum reflectivity in the ultraviolet, a 52-mm-diam beam splitter feeding two individual fiber optics, relay lenses, interference filters, and photomultipliers. All optical components were quartz to give good transmission in the near UV wavelengths. The optical axis of the primary lens was inclined at 7 deg to the tangent to the model surface at the point where the beam emerged to avoid optical cut-off at points close to the surface. The optical splitter divided the light from the beam into two paths. In each path, at the point where the beam image was focused by the primary lens, a slit was formed by a fiber optic in which the fibers had

been flattened into a narrow band. The light thus selected from a small portion of the fluorescing beam was channeled to one of the two photomultipliers housed outside the test section. With this system two small segments of the beam could be viewed simultaneously and traversing mechanisms were provided to vary the sample points independently. The optical equipment was mechanically very stiff to combat the vibrations that are inevitable with intermittent wind tunnels. The photomultiplier outputs were amplified by either Keithley electrometer amplifiers with a bandwidth dc to 100 KHz or a somewhat faster amplifier constructed within the laboratory. Signals were stored within the laboratory digital data system which is capable of 2×10^6 samples per second.

Efforts to improve the electrical and optical performance of the equipment highlighted fundamental limitations that arise from the mechanism of the photometry. To achieve a high spatial resolution, light can only be gathered from a small volume of the weakly fluorescing beam. As a consequence the photon fluxes are low and the average frequency at which photons arrive at the photomultiplier may be close to the upper 10^5–10^6 Hz band where signals from the smaller scale turbulence can be expected. Thus, inherent problems may be encountered because of poor signal-to-noise ratios. Nevertheless it has been shown that, with the technique, it is possible to obtain detailed measurements of the fluctuating density within a hypersonic boundary layer. Results with unattenuated frequency components up to 10^5 Hz were achieved with a spatial resolution of 0.13 mm in the beam direction. In the direction perpendicular to this the resolution varied from 0.1 mm to 0.6 mm. An improved optical system would have extended the range to 10^6 Hz.

Results and Discussion

Velocity-Temperature Correlations

Boundary-layer pitot profiles were obtained at four stations, i.e., x = 520, 620, 720, and 820 mm. The static surface pressure distribution was measured at 13 positions along a cone generatrix and showed a slight (1.3% in 0.4 m) favorable pressure gradient. The total temperature profiles were measured only at the third and fourth stations (x = 720 mm and x = 820 mm).

In order to compare theoretical and experimental velocity temperature correlations, both velocity and temperature profiles were obtained from the Mach number and total temperature profiles at stations 3 and 4. The Mach number profiles were calculated from the Rayleigh supersonic pitot formula. The velocities were then calculated using the relationship

$$\frac{u}{u_e} = \frac{M}{M_e}\left[\frac{T_o}{T_{oe}}\frac{[1 + \tfrac{1}{2}(\gamma - 1)M_e^2]}{[1 + \tfrac{1}{2}(\gamma - 1)M^2]}\right]^{-\frac{1}{2}} \tag{1}$$

The temperature profiles were obtained using

$$T = T_o - u^2/2c_p \tag{2}$$

The measured results were compared with the van Driest modification of the Crocco relationship

$$\frac{T}{T_e} = \frac{T_w}{T_e} + \frac{(T_r - T_w)}{T_e}\frac{u}{u_e} - r\frac{(\gamma - 1)}{2}M_e^2\left(\frac{u}{u_e}\right)^2 \tag{3}$$

where

$$T_r = T_e\{1 + r[(\gamma - 1)/2]M_e^2\}$$

$$r = 0.89$$

Agreement (see Fig. 1) is close for the outer part of the layer whereas towards the wall the measured values fall lower than the prediction. Closer agreement was shown in the density measurement, which will be seen later. As total temperature data were not available for the two forward measuring stations, it was thought that it was a reasonable assumption for this near-zero pressure gradient situation to calculate these velocity profiles from the Mach number profiles using the modified Crocco relationship.

Fitting the velocity data to a power law of the form

$$u/u_e = (y/\delta_u)^{1/N} \tag{4}$$

where δ_u is defined as the point from where $u = 0.995u_e$, yields values of N that increase from about 7.4 at the furthest forward station to 10.4 at the last station. Other integral quantities are shown in Table 1.

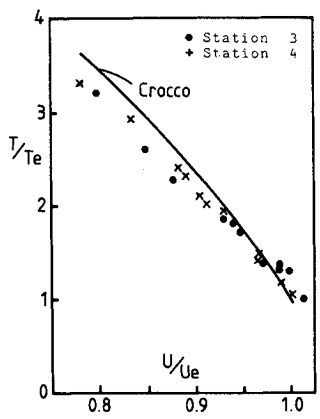

Fig. 1 Velocity-temperature relationship.

Table 1 Integral quantities

Station	1	2	3	4
x mm	520	620	720	820
θ mm	0.133	0.147	0.161	0.177
δ_u mm	3.78	4.34	4.79	5.55
δ_p mm	4.94	5.64	6.34	7.22
$Re_e/m \times 10^7$	6.63	6.44	6.26	6.16
$Re_e \times 10^7$	3.44	3.99	4.50	5.05
Re_θ	8820	9470	10070	10900
δ^* mm	2.27	2.51	2.72	2.99
δ_3 mm	0.239	0.265	0.289	0.315
δ_4 mm	0.103	0.113	0.124	0.135
H_{12}	17.1	17.1	16.9	16.9
H_{32}	1.80	1.80	1.80	1.78
H_{42}	0.77	0.77	0.77	0.76

Reynolds Analogy Factor

Heat transfer was measured at 11 positions along the cone surface covering the region where the pitot pressure surveys were made. From these data, local Stanton numbers were calculated. Surface impact pressure was measured with Preston tubes at six positions along the cone surface. Skin friction coefficients were evaluated using the methods of Sigalla,[3] Hopkins and Keener,[4] Allen,[5] Patel,[6] and Fenter and Stalmach.[7] All gave similar predictions of C_f for the different-sized tubes and measuring stations and an average value was used. The scatter was about 7%.

In this near equilibrium region, C_f changed more slowly than in the transition zone, and the expected slight fall in C_f could not be resolved as it was within the experimental scatter. Averaging all the data from six measuring stations yielded a mean value for C_f of 8.90×10^{-4}. Heat transfer values for all measuring stations were also nearly constant and, after averaging, yielded a mean Stanton number of 4.7×10^{-4}. This agreed well with enthalpy defect data. A Reynolds analogy factor of 1.05 was obtained.

Cole's Law

Velocity values were reduced to $\bar{u}^*/u_e$ by the use of the van Driest transformation

$$\frac{\bar{u}^*}{u_\tau} = \frac{1}{A\sqrt{(C_f/2)(T_w/T_e)}}\left[\sin^{-1}\left(\frac{2A^2(u/u_e)-B}{\sqrt{4A^2+B^2}}\right) + \sin^{-1}\left(\frac{B}{\sqrt{4A^2+B^2}}\right)\right] \tag{5}$$

where

$$A = \sqrt{(T_e/T_w)[(\gamma-1)/2]M_e^2}$$

$$B = [(T_e/T_w) + A^2 - 1]$$

The four transformed profiles have been plotted against yu_τ/ν_w in Fig. 2. Also shown are the lines indicating Cole's Law of the Wall,

$$\frac{\bar{u}^*}{u_\tau} = \frac{1}{k}\ell n\left(y\frac{u_\tau}{\nu_w}\right) + c \tag{6}$$

where $k = 0.40$ and $c = 5.1$.

From the profiles it is clear that as the Reynolds number increases, there is better agreement with Cole's Law. At the third and fourth measuring stations there are substantial regions where the measured data lies close and parallel to Cole's Law. These changes are symptomatic of a very gradual development of the boundary layer towards an equilibrium turbulent state following transition.

Wake Component

The wake components for the outer region of the layer are less than the values obtained from Cole's relationship for incompressible turbulent boundary layers. However, the measurement of this requires extreme accuracy since it involves the differences between velocities that are similar in magnitude. It is apparent that most of the published data for this component obtained in the supersonic regime are scattered.

Defect Law

Maise and McDonald[8] have attempted to extend the validity of the van Driest transformation to the outer layer by the introduction of u^* into the velocity defect law with a finite wake component

$$\frac{\bar{u}_\delta^* - \bar{u}^*}{u_\tau} = -2.5\ell n(y/\delta_p) + 1.25(2-w) \tag{7}$$

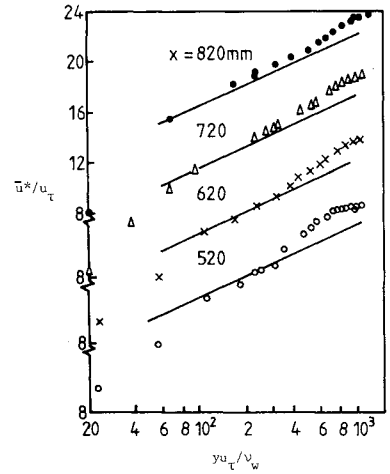

Fig. 2 Velocity profiles using Cole's Law.

where $w = 1 - \cos(y/\delta_p)$. This concept works satisfactorily for adiabatic supersonic boundary layers, but it has been found to fail if the wake component has not fully developed. Fernholz[1] has achieved better correlations for nonadiabatic data using the semiempirical relationship

$$\frac{\bar{u}_\delta^* - \bar{u}^*}{u_\tau} = -4.70\ell n(y/\Delta^*) - 6.74 \tag{8}$$

where

$$\Delta^* = \delta_p\int_0^1 \frac{\bar{u}_\delta^* - \bar{u}^*}{u_\tau}\,\mathrm{d}(y/\delta_p)$$

The new length scale parameter Δ^* is introduced to deal with the problem of evaluating a boundary layer thickness in the compressible flow. Comparisons are shown in Fig. 3, and all four measured profiles are close to the line predicted by Fernholz.

Turbulent Shear Stress

By integrating the momentum equation in the y direction from the wall to a given position inside the boundary layer, the total shear stress can be obtained as

$$\frac{\tau r}{\rho_e u_e^2} = r_o\frac{C_f}{2} + \left(\frac{\mathrm{d}\delta}{\mathrm{d}x} + \frac{\delta}{x}\right)\cdot\int_0^{y/\delta}\left(1+\frac{y}{r_o}\right)\frac{\rho}{\rho_o}\left(\frac{u}{u_e}\right)^2\mathrm{d}\left(\frac{y}{\delta}\right) - \left(\frac{\mathrm{d}\delta}{\mathrm{d}x} + \frac{\delta}{x}\right)\left[\frac{u}{u_e}\int_0^{y/\delta}\left(1+\frac{y}{r_o}\right)\frac{\rho u}{\rho_e u_e}\mathrm{d}\left(\frac{y}{\delta}\right)\right] + \frac{y}{\rho_e u_e^2}\frac{\partial p}{\partial x} \tag{9}$$

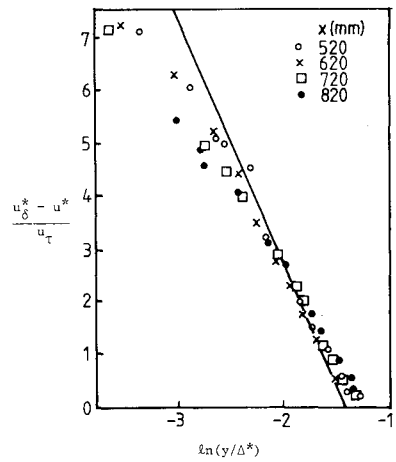

Fig. 3 Defect law.

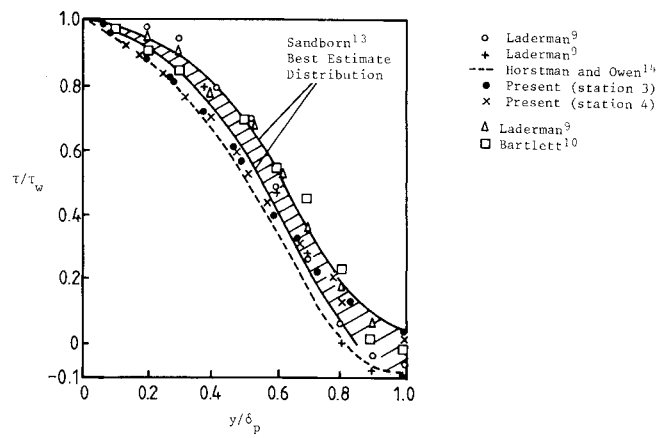

Fig. 4 Comparison of total shear stress distributions (after R. P. Bartlett[10]).

Except in the viscous sublayer and buffer layer, the total shear stress can be regarded as equal to the turbulent shear stress. For the sharp cone with a constant wall temperature, a near-equilibrium state was achieved by the time the flow had reached stations 3 and 4 ($x = 720$ and 820 mm respectively) and little variation with x in the normalized profiles is seen. Figure 4 shows the total shear stress distributions for these stations compared with other published data obtained at very different flow conditions. If there is any consistent trend in the sensitivity of the distributions to Mach number, Reynolds number, or wall temperature, it is not apparent, or it is masked by experimental error.

Mixing Length and Eddy Viscosity Distributions

Although the concepts of mixing length and eddy viscosity are suspect for analyzing the boundary layer under consideration, their values can be calculated from the following relationships.

$$\frac{\ell}{\delta_p} = \frac{\tau_t/\rho_e u_e^2}{[\rho/\rho_e \partial(u/u_e)/\partial(y/\delta)]^{1/2}} \tag{10}$$

In the present case:

$$\ell \simeq \begin{cases} 0.4y; & y \le 0.1\delta_p \\ 0.072\delta_p; & 0.3\delta_p \le y \le 0.6\delta_p \end{cases}$$

and

$$\ell/\delta_{p(\text{maximum})} \simeq 0.074 \text{ when } y = 0.4 - 0.45\delta_p$$

Values of the mixing length calculated for stations 3 and 4 show that the distribution is close to that for a low-speed turbulent boundary layer. The eddy viscosity can be obtained from the velocity profiles using the formula

$$\frac{\epsilon}{u_e \delta_i^*} = \frac{\tau_t/\rho_e u_e^2}{(\rho/\rho_e)\,\partial(u/u_e)/\partial(y/\delta)\,(\delta_i^*/\delta)} \tag{11}$$

where

$$\delta_i^* = \int_0^\delta (1 - u/u_e)\, dy$$

$u_e\delta_i^*$ is used in an attempt to collapse the data for different M_e and Re. The present results for stations 3 and 4 are shown in Fig. 5 compared with some of the available data. Good agreement is found with Laderman's[9] and most of Bartlett's[10] data obtained in a similar experiment at lower Reynolds number.

Mean Density

The values of the mean density were deduced from observation of the intensities of fluorescence produced along the electron beam as it traversed through the boundary layer. These were made at the rearmost measuring station only ($x = 0.820$ m). Iterative calculations, which take into account that attenuation of the beam current as it passed through the gas, were performed to obtain the density. The formula used, which was deduced from calibration experiments on the beam, was

$$S \equiv \frac{V_s}{ig} = \frac{4.19\rho + 6.34 \times 10^{-3}\rho^2}{1 + 1.80 \times 10^{-2}\rho(T/T_{\text{room}})^D} e^{-KQ} = R(\rho)e^{-KQ} \tag{12}$$

where

$$Q = \int_0^\ell \rho(\ell)\, d\ell, \quad K = 3 \times 10^{-4} \text{ and } D = 0$$

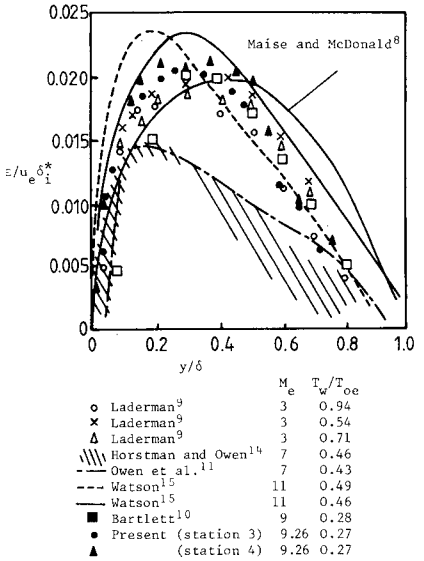

Fig. 5 Eddy viscosity profiles (after R. P. Bartlett[10]).

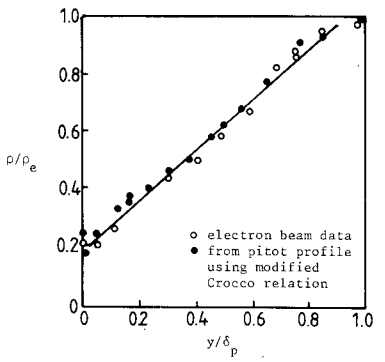

Fig. 6 Mean density profiles.

Here, V_s, i, g, and ℓ are the photomultiplier voltage output, the beam current, the gain of the system, and the length measured along the beam from the point it entered the test gas, respectively. Measured values of the mean density are shown in Fig. 6 compared with those inferred from the pitot and total temperature probe surveys reduced using the Crocco T-u relationship. The expected accuracy of the present results is estimated to be ±5%, and the agreement between the two sets of data can be seen to be very good.

Distribution of RMS Density Fluctuations

The influence of beam attenuation resulting from the accumulative effect of density fluctuation along its path could not be determined in our experiment. However, since the fluctuations were about an order of magnitude less than the mean value of the density, and the second derivative of the relationship between density and beam intensity were small over the measuring range, we can write

$$\tilde{\psi}_\rho = \frac{R(\rho)}{dR(\rho)\, d\rho}\, \tilde{\psi}_s \tag{13}$$

where $\tilde{\psi}_x$ indicates the ratio of the rms value of the fluctuating component x', of a quantity x, and the mean value $\bar{x}$. The errors thus incurred were thought to be insignificant.

The measured density fluctuations are plotted in Fig. 7 where they are compared with other available data. These show a great deal of variation although it should be pointed out that the other experiments cover a very considerable range of test

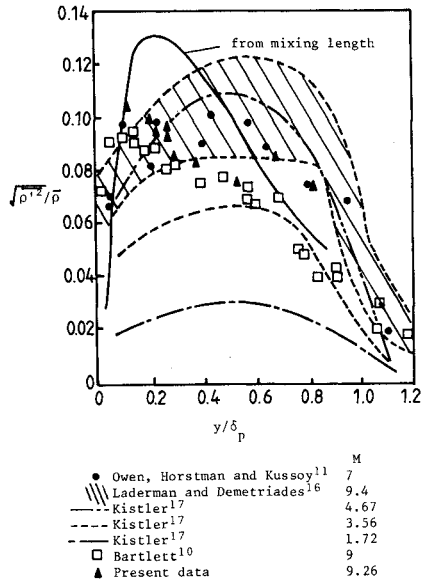

Fig. 7 Fluctuating density compared with results using hot-wire anemometry.

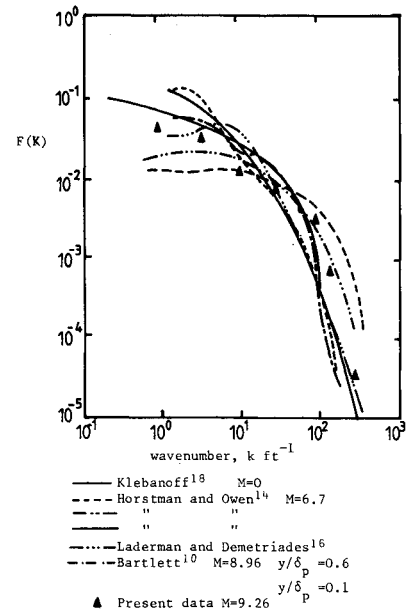

Fig. 8 Averaged spectral density profiles compared with available data.

conditions. Close agreement has been obtained with Bartlett's experiment performed in the same wind tunnel with a tripped boundary layer at lower Reynolds number and with the $M = 7$ data of Owen et al.[11]

Several authors have used a mixing length concept to model the fluctuating density for a compressible boundary layer. This can be written as

$$\tilde{\psi}_\rho = \frac{\ell}{\delta_p}\frac{\rho_e}{\rho}\frac{\mathrm{d}(\rho/\rho_e)}{\mathrm{d}(y/\delta_p)} \tag{14}$$

and, as all of the quantities on the right-hand side of this equation have been measured, we are in a position to verify whether or not this concept is useful. The calculated values using Eq. (14) have been added to Fig. 7. It can be seen that the mixing length model only very approximately predicts the fluctuation levels, overestimating these for $0.2 < y/\delta_u < 0.5$ and underestimating beyond this. Nevertheless for rough calculations of hypersonic boundary layers the simple mixing length model may be of some limited value.

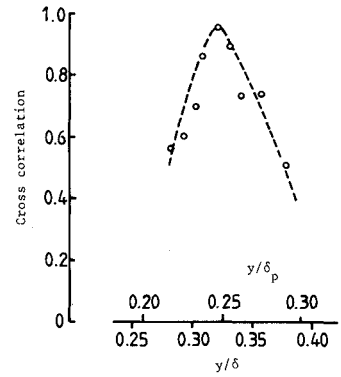

Fig. 9 Cross correlation along the electron beam axis.

Power Spectral Densities

A number of tests were performed in which records were made of the fluctuations in beam intensity sensed by the two photomultipliers. From these, spectra and auto- and cross-correlations were computed (see Lin and Harvey[12]). A few of these results are included here. The fluctuations in density were measured at six different locations throughout the boundary layer from $y/\delta_p = 0.11$ to 0.85. The output from the photomultipliers was filtered to improve the signal-to-noise ratio but was unattenuated below 1×10^5 Hz. From this the spectral density function $F(K)$ as a function of wave number K, i.e.,

$$F(K) = (u/2)p(f); \quad K = 2\pi f/u \tag{15}$$

is calculated, where $p(f)$ is the power spectral density and u the local flow velocity. Since each record represents only a few milliseconds of test time there is some statistical uncertainty in the results at the lower frequencies. However, the individual spectra are very similar, and averaging all sets of data yields a mean spectral density function, which has been plotted in Fig. 8, where it is compared with other available results. Although there is much scatter in these curves, there appears to be some evidence for a systematic difference between the hypersonic spectra and the curve for $M = 0$. At hypersonic speed, $F(K)$ is lower than the incompressible result at low wave numbers and higher at values around 0.3×10^2 m^{-1}. The results of Bartlett obtained in a tripped boundary layer that showed strong transitional characteristics contradict this.

Correlation Measurements

Autocorrelations were calculated for two sets of measurements made at $y/\delta_p = 0.53$ and 0.83 (see Lin and Harvey[12]). Spatial correlation and coherence measurements of density were also made by traversing the observation point of one photomultiplier while keeping the other fixed. Using the same argument employed above, it can be shown that the correlation can be calculated to good accuracy from the observed signals S_1 and S_2.

The fixed detector was focused at a point $y = 1.80$ mm, which corresponds to $y/\delta_p = 0.249$ ($y/\delta_u = 0.324$). It should be noted that the line along which this correlation was measured was the path of the electron beam that was inclined at 40 deg normal to the cone surface. The results, which are shown in Fig. 9, therefore include an element of longitudinal correlation.

The sharpness of the peak indicates that there is significant energy in the small eddies at high wave numbers. Judging from fitting an osculting parabola these eddies would have an inferred scale of the order of 0.01 mm that is just below the limit of the resolving power of the detection system. These eddies could therefore be even smaller.

The coherence between pairs of signals obtained for different values of y was also calculated. As expected, these signals only correlate at the lower wave numbers corresponding to the larger eddies, and the frequency at which this begins to fall off is progressively lower as the distance between the two measuring stations is increased. At the maximum separation of the detectors (which was $+0.041\delta_p$ and $-0.031\delta_p$), the signals were correlated up to about 1.6 KHz ($K \simeq 11$ m^{-1}).

Conclusions

In this study, results have been obtained using an electron beam as the diagnostic tool to probe a hypersonic turbulent boundary layer. The technique has been used at a density and hence Reynolds number higher than hitherto thought practical. This has been made possible by adopting a novel method of isolating the electron gun from the test flow. Calibration tests have demonstrated that the electron beam technique can be used in flows where the equivalent room-temperature pressure is 110 Torr.

Useful mean and turbulent data have been obtained for a naturally turbulent hypersonic boundary layer on a sharp 5 deg cone at zero incidence, using conventional and electron beam fluorescence techniques. Limited total temperature measurements indicate that the Crocco temperature distribution is an appropriate assumption for this near-zero pressure-gradient boundary layer. The measurement of the mean density distribution agrees with the profile that was inferred from the total temperature and pressure surveys reduced using the Crocco relationship. This is, in some ways, surprising since the Crocco expression is thought to be suspect in the present flow situation. The experiment would suggest otherwise. However, no case is being made for the use of the Crocco relationship in situations other than those of the present observations. The velocity profiles that were calculated using this relationship show that the turbulent boundary layer has a substantial and changing wake component indicating a history effect following transition. It would appear that the outer part of the layer achieves its "turbulent state" earlier than the inner part. Calculations of the distribution of turbulent shear stress and eddy viscosity suggest that there is little fundamental difference between this Mach 9 layer and lower speed flows. However, this may be a misleading conclusion that generally cannot be applied to non-zero pressure gradient layers since it is thought that the growing importance of fluctuations in the temperature and density will give rise to a change in the physical structure of the layer.

Measurements through the layer show that the turbulence level in terms of density fluctuations is moderately constant falling roughly from 11% at $y/\delta_p = 0.11$ to 8% at $y/\delta_p = 0.85$. This is in contrast to the expected behavior predicted by the simple mixing length concept. Spectra exhibit similar trends to those reported in other experiments on hypersonic layers and show marked differences to the results from incompressible flows in being lower at low wave number and higher at high wave number. Auto- and cross-correlation measurements both emphasize that there is considerable energy in the small eddies (those of the scale less than about $0.02\delta_p$).

Acknowledgments

The help given by Dr. R. Hillier and Mr. Z. H. Wang who supplied the total temperature data is gratefully acknowledged. The work was carried out with the support of the British Ministry of Defence under Agreement AT/2037/084.

References

[1]Fernholz, H. H., "Compressible Turbulent Layers," *Von Kármán Institute Lecture Series,* No. 86, VKI, Brussels, 1976.

[2]Wang, Z. H. and Hillier, R., "The Measurement of Total Temperature Profiles in the Hypersonic Turbulent Boundary Layer on a Cone Immersed in a $M = 9.26$ Flow," Imperial College, London, Aero Rept. 82-102, May 1982.

[3]Sigalla, A., "Calibration of Preston Tubes in Supersonic Flow," *AIAA Journal,* Vol. 3, Aug. 1965, p. 1531.

[4]Hopkins, E. J. and Keener, E. R., "Study of Surface Pitot Tubes for Measuring Turbulent Skin Friction at Supersonic Mach Numbers—Adiabatic Wall," NASA TN-D-3478, 1966.

[5]Allen, J. M., "Re-Evaluation of Compressible Flow Preston Tube Calibrations," NASA TM-X-3488, 1977.

[6]Patel, V. C., "Calibration of the Preston Tube and Limitations on its Use in Pressure Gradients," *Journal of Fluid Mechanics,* Vol. 23, Sept. 1965, p. 185.

[7]Fenter, F. W. and Stalmach, C. J., "The Measurement of Local Turbulent Skin Friction at Supersonic Speeds by Means of Surface Impact Pressure Probes," Univ. of Texas, Austin, TX, Rept. DRL-392, Oct. 1957.

[8]Maise, G. and McDonald, H., "Mixing Length and Kinematic Eddy Viscosity in a Compressible Boundary Layer," *AIAA Journal,* Vol. 6, Jan. 1968, p. 73.

[9]Laderman, A. J., "Effect of Wall Temperature on a Supersonic Turbulent Boundary Layer," *AIAA Journal,* Vol. 16, July 1978, p. 723.

[10]Bartlett, R. P., "A Study of Mean and Fluctuating Properties of a Turbulent Hypersonic Boundary Layer," Univ. of London, Ph.D. Thesis, 1981; also Bartlett, R. P. and Harvey, J. K., "Electron Beam Measurements of the Density in a Hypersonic Turbulent Boundary Layer at $M = 9$," Imperial College, London, Aero Rept. 80-01, Jan. 1980.

[11]Owen, F. K., Horstman, C. C., and Kussoy, M. I., "Mean and Fluctuating Flow Measurements of a Fully Developed, Non-Adiabatic Hypersonic Boundary Layer," *Journal of Fluid Mechanics,* Vol. 70, July 1975, p. 393.

[12]Lin, Z. B. and Harvey, J. K., "The Investigation of the Structure of Hypersonic Turbulent Boundary Layers on a 5° Sharp Cone Using the Electron Beam Fluorescence Technique," Imperial College, London, Aero Rept. 82-02, 1986.

[13]Sandborn, V. A., "A Review of Turbulence Measurements in Compressible Flow," NASA TM-X-62-337, 1974.

[14]Horstman, C. C. and Owen, F. K., "Turbulent Properties of a Compressible Boundary Layer," *AIAA Journal,* Vol. 10, Nov. 1972, p. 1418.

[15]Watson, R. D., "Wall Cooling Effects on Hypersonic Transitional/Turbulent Boundary Layers at High Reynolds Numbers," *AIAA Journal,* Vol. 15, 1977, p. 1455.

[16]Laderman, A. J. and Demetriades, A., "Mean and Fluctuating Flow Measurements in the Hypersonic Boundary Layer Over a Cooled Wall," *Journal of Fluid Mechanics,* Vol. 63, March 1974, p. 121.

[17]Kistler, A. L., "Fluctuation Measurements in a Supersonic Turbulent Boundary Layer," *Physics of Fluids,* Vol. 2, May–June 1959, p. 290.

[18]Klebanoff, P. S., "Characteristics of Turbulence in a Boundary Layer with Zero Pressure Gradient," NACA Rept. 1247, 1955.